International Journal of Fracture **82:** 297–316, 1996.
© 1996 *Kluwer Academic Publishers. Printed in the Netherlands.*

Fracture statistics applied to modelling the non-linear stress–strain behavior in microcomposites: Influence of interfacial parameters

L. GUILLAUMAT and J. LAMON
Laboratoire des Composites Thermostructuraux, UMR 47 (CNRS-SEP-UB1), Domaine Universitaire, 3 Allée de La Boétie, 33600 Pessac, France

Received 13 February 1996; accepted in revised form 25 October 1996

Abstract. A model is proposed for predicting the non-linear stress-strain relations and ultimate failure of microcomposite specimens as a function of interfacial characteristics. The description of the matrix cracking process and fiber failure is based on fracture statistics. The microcomposite specimen consists of a single fiber coated with concentric layers of interfacial material and matrix. It is representative of the constituents in the actual composite and is appropriate for designing interphases.

This approach was applied to practical SiC/SiC microcomposites specimens made by Chemical Vapor Deposition. The predictions of matrix cracking compare satisfactorily with experimental data. Important trends in the influence of interfaces upon the stress–strain behavior are thus predicted and discussed in relation to available experimental results.

Key words: ceramic-matrix composites, microcomposites, tensile behavior, matrix fragmentation, fracture statistics, failure, interfaces.

1. Introduction

It is now well acknowledged that the fiber/matrix interfacial region exerts a profound influence on the mechanical response of ceramic matrix composites (CMCs). The effect of interphase (i.e. fiber coating) properties and interfacial damage on the stress–strain response has been evidenced by several experimental studies on 1D [1] and 2D [2, 3] composites and on microcomposites [4]. Therefore, it may be expected that composites could be tailored as a function of end use applications, provided that quantitative relations between mechanical behavior and interphase characteristics are established.

Fiber/matrix interphases favor crack deflection, eventual further matrix cracking and fiber pull-out. A dense network of matrix cracks is created in the presence of rather strong fiber/matrix interactions and limited interfacial damage [3, 5] whereas fiber pull-out requires rather weak fiber/matrix bonding. The former effect is preferred in 2D CVI composites whereas the latter phenomenon seems to be recommended by authors for a variety of 1D composites. High stresses and a high toughness have been measured on 2D SiC/SiC CVI-composites possessing rather 'strong' interphases [3, 5]. The related tensile stress–strain curves exhibit typical features. In the presence of weak fiber/matrix interfacial regions, a plateau-like stress–strain behavior is obtained (Figure 1): the non-linear domain attributed to matrix cracking extends over a narrow range of stresses and strains and the stress at matrix cracking saturation is distinct from ultimate strength. In contrast, in the presence of rather strong interphases, the stresses are higher, the non-linear domain is wider and the stress at saturation is now close to or coincides with ultimate strength (Figure 1).

There have been several attempts in the literature directed at predicting the basic features of the tensile stress–strain response of CMCs. Most studies have been mainly concerned

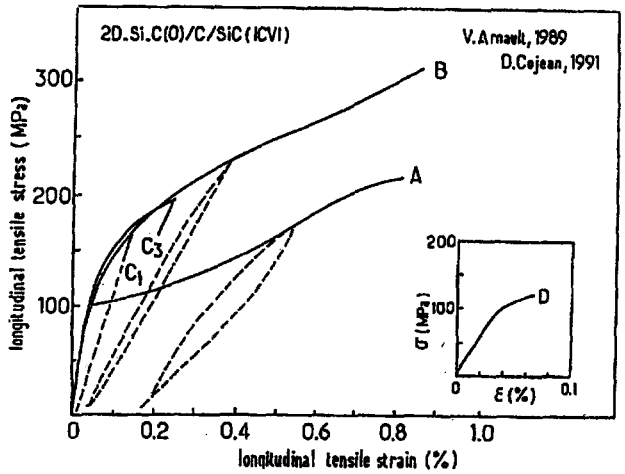

Figure 1. Schematic diagram showing the typical tensile stress–strain behaviors which are observed with current 2D woven SiC/SiC composites: (A) weak interphase, (B) strong interphase, (D) no interphase [2].

with the failure and toughness aspects [6–11]. Aveston, Cooper and Kelly were the first to provide a closed form equation for the first critical matrix cracking strain [6]. Then, a number of micromechanics-based analyses have been developed for predicting the onset of matrix cracking, taking into account various fiber/matrix interactions [7–9]. A number of theories of ultimate strength have also been proposed for unidirectional ceramic matrix composites [12–15]. Relatively little effort has been devoted to the subsequent accumulation of matrix cracks and the associated non-linear stress–strain response prior to failure. Few attempts are directed at predicting the effect of interfacial damage [16] or interfacial shear stress [17] on stress–strain response. They are restricted to considering a uniformly degraded interphase [16] or a uniform crack spacing [17], neglecting the random defect-induced aspect of cracking in brittle matrices.

The primary purpose of this present paper is, therefore, to establish a model which describes the influence of interfacial damage on matrix cracking and on the associated stress–strain response of *microcomposite specimens*. Fiber/matrix interphase characterstics expressed in terms of a shear stress or a debond length. Formation of matrix cracks and fiber failure are described using strength-probability equations derived from statistical approaches to brittle failure. This approach differs from the conventional one which considers the total volume of cracked material. In paper, matrix cracking is described as the brittle failure of uncracked volume elements (matrix fragments). This allows one to solve problems involving non-uniform stress-states. The model was then applied to predict the stress–strain behavior of practical SiC/SiC microcomposite specimens made by Chemical Vapor Deposition (CVD).

The microcomposite specimen consists of a concentric cylinder element containing a single fiber, with a coating (i.e. the interphase) plus a matrix annulus (Figure 2). It is representative of the constituents of the actual composite fabricated by using identical vapor deposition conditions. The microcomposite configuration is appropriate for designing interphases. Tension experiments on microcomposite test specimens are currently used for investigating fiber/matrix interactions and their influence upon matrix cracking, ultimate fracture and the associated stress–strain relations [4, 18–22]. The procedures used for producing and testing these specimens, as well as for extracting interfacial characteristics from experimental load

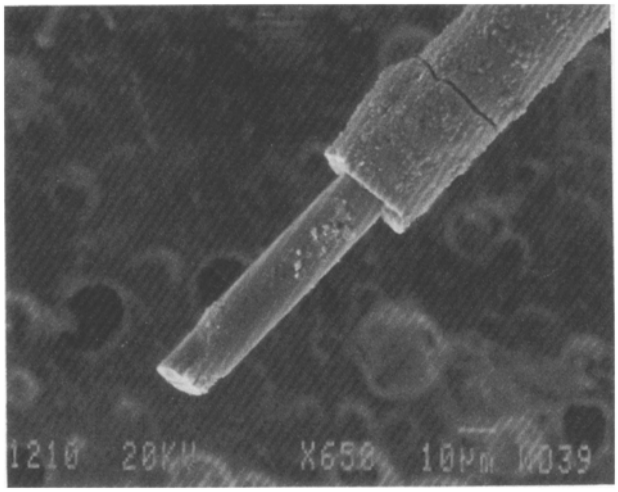

Figure 2. Scanning Electron Micrograph of a microcomposite test specimen which failed under tension showing the Carbon coating on the surface of the pulled out fiber as well as a matrix fragment delineated by two transverse cracks.

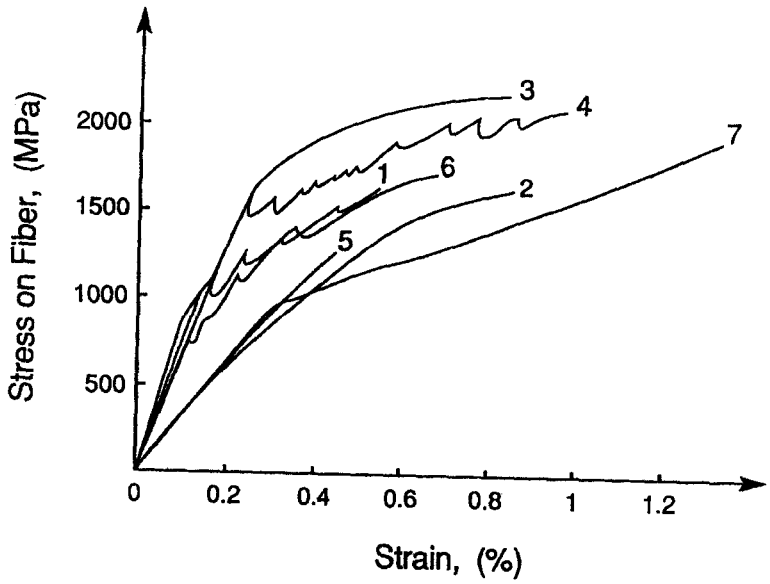

Figure 3. Typical tensile stress–strain curves measured on various batches of SiC/BN/SiC microcomposite test specimens with a range of interphases. The numbers identify the batches. The interphases were rather weak in batches 1, 4, 6 and 7, whereas they were stronger in batches 2, 3 and 5. The volume fraction of the matrix was smaller in batches 2, 5 and 7. The stress refers to that acting on the fiber at the location of matrix cracks.

displacement curves have been described elsewhere [4, 18–20, 22]. The tensile load displacement curves exhibit the typical features previously discussed with practical CMCs: non linearity induced by matrix cracking and debonding, and an eventual linear domain dominated by matrix crack opening and fiber deformations. The load-displacement curves obtained for various microcomposite specimens are summarized in Figure 3.

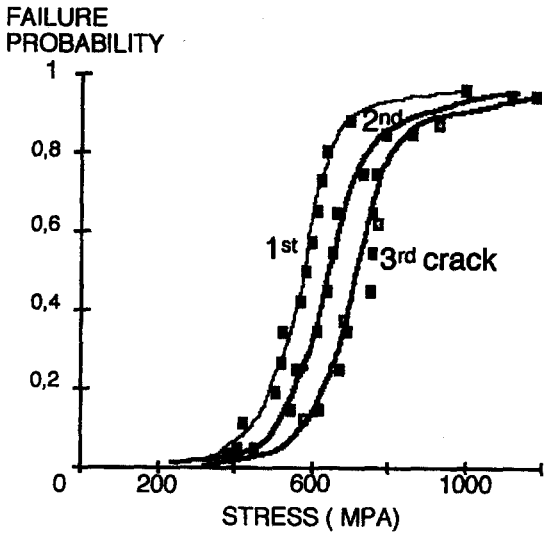

Figure 4. Statistical distributions of matrix cracking stresses measured on SiC/C/SiC microcomposites (gauge length = 10 mm) [4].

2. Analytical relationships

Experiments show that in a microcomposite test specimen loaded in tension parallel to the fiber axis, transverse cracks form sequentially in the matrix at increasingly applied stresses. Each crack propagates unstably through the matrix and perpendicular to the fiber, and then deflects in the fiber/matrix interphase. The matrix thus becomes subdivided into fragments which are like tubes in shape (Figure 2). The fragments are thus *uncracked* volume elements. They become smaller and smaller as cracking proceeds. Features of the matrix cracking process are reflected by the non-linear domain of the load-displacement curves (Figure 3) and by acoustic emission recorded during tensile tests [4, 18, 22].

It is worth pointing out that matrix cracking involves the *brittle failure* of matrix fragments and that each new crack in the matrix is the result of the brittle failure of an uncracked fragment of given volume. Weakest link statistics are appropriate for describing the brittle failure of a matrix fragment. The *brittle failure of a matrix fragment* as well as the fracture of the fiber are probabilistic-statistical events as a result of the presence of flaw populations. They are characterized by statistical distributions of stress data [4, 19]. Figure 4 shows an example of the statistical distributions of strength data pertinent to the matrix fragments generated by the first and the second cracks in SiC/SiC microcomposites under tension. The strength increase with the number of cracks results from the decrease in the volume of fragments. Such scale effects are now well established in brittle ceramics. They are described using statistical-probabilistic approaches. In paper, the Weibull approach is applied to the brittle failure of the uncracked matrix fragments and the fiber in microcomposites subject to uniaxial tensile loading conditions. This approach thus differs from the conventional one which considers the total volume of cracked material. It takes into account the stress gradients induced by the fiber/matrix interactions. The Weibull approach provides a satisfactory approximation in the presence of essentially uniaxial stress-states.

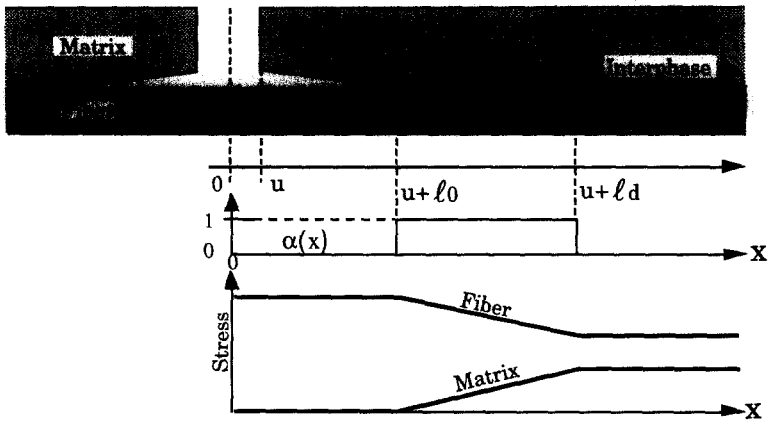

Figure 5. Schematic diagram showing the local stress-states induced in the fiber and in the matrix by a matrix crack; also shown is the function $\alpha(x)$ appearing in Equation (1).

2.1. INTERFACIAL DAMAGE

Debonding caused by the deflection of matrix cracks into the interphase locally affects the applied stress-field, inducing stress gradients in the fiber and in the matrix as exemplified by Figure 5 for a constant interfacial shear stress. Stresses in the fiber are maximum over the distance $(u+l_0)$, where u is the crack opening displacement and l_0 is the distance along which Poisson's effect is dominant.

The following equation was used to describe the shear stress τ along the interface taking into account the contribution of the applied stress-dependent phenomena:

$$\tau(x) = (\tau_0 + k\sigma)\alpha(x), \tag{2.1}$$

where τ_0 is the interfacial shear resistance, σ is the remote stress applied to the microcomposite, k is a coefficient accounting for the stress-dependent fiber/matrix interactions in the debond portion involving friction, residual stresses and Poisson's effect. $k > 0$ when compression is dominant, $k < 0$ when residual tension is dominant. The function $\alpha(x)$ allows one to take into account the Poisson's effects. In this paper, a step function[1] was selected for $\alpha(x)$ (Figure 5), thus subdividing the matrix fragments into three different regions in the vicinity of the cracks:

(i) Region 1: Poisson's effect; $\alpha(x) = 0$ and $\tau(x) = 0 (0 < x < u + l_0)$
(ii) Region 2: sliding friction; $\alpha(x) = 1$ along the debond $(u + l_0 < x < u + l_d)$
(iii) Region 3: undamaged interphase $(x > u + l_d)$

The determination of the stress field in Regions 1 and 2 is straightforward. The stress field in Region 2 was derived from the following equations of equilibrium:

$$\frac{d\sigma_F}{dx} = -\frac{2}{r_F}\tau \qquad \frac{d\sigma_M}{dx} = \frac{2}{r_F}\tau\left(\frac{V_F}{1-V_F}\right), \tag{2.2}$$

where σ_F and σ_M are the stresses operating on the fiber and the matrix respectively; r_F is the fiber radius; and V_F is the volume fraction of fiber.

[1] Any functional form for $\alpha(x)$ may be considered

Integrating Equations (2) leads to the following relations for σ_F and σ_M along the debond:

$$\sigma_F(\mathbf{x}) = \frac{\sigma}{V_F}\left(1 - \frac{a}{1+a}\cdot\frac{\mathbf{x}-u-\ell_0}{\ell_d-\ell_0}\right) \quad x \geqslant u+\ell_0 \tag{2.3}$$

$$\sigma_M(x) = \frac{\sigma}{1-V_F}\cdot\frac{a}{1+a}\cdot\frac{x-u-\ell_0}{\ell_d-\ell_0} \quad x \geqslant u+\ell_0, \tag{2.4}$$

where $\sigma = F/A_\mu$ (F is the applied force and A_μ is the microcomposite cross sectional area), and $a = (E_M(1-V_F)/E_F V_F)$ (E_M and E_F are moduli of the matrix and the fiber respectively).

The debond length as a function of the applied stress (Equation (6)) is derived from the following particular values of Equation (3) at the boundaries of Region 2 of the matrix fragments

$$\sigma_F(u+l_0) = \frac{\sigma}{V_F}, \qquad \sigma_F(u+l_d) = \frac{\sigma}{V_F(1+a)}, \tag{2.5}$$

$$l_d = \frac{\sigma.a.r_F}{2.V_F.(1+a).(1-\beta).(\tau_0+k\sigma)} \quad \text{where } \beta = \frac{\ell_0}{\ell_d}. \tag{2.6}$$

2.2. Stress–strain relationships

Deformations of the microcomposite were determined from fiber elongations in the regions delineated by the debond.

In the presence of a single crack, fiber elongation in the vicinity of the debond (including Regions 1 and 2) was derived from the stress state.

$$U_F(\sigma) = \int_0^{u+\ell_d} \frac{\sigma_F}{E_F}.\mathrm{d}x \tag{2.7}$$

Integration of Equation (7) gives:

$$U_F(\sigma) = \frac{\sigma.\ell_d}{E_F.V_F}.\left[\frac{u}{\ell_d} + 1 - \frac{a.(1-\beta)}{2.(1+a)}\right]. \tag{2.8}$$

A similar analysis leads to the following equation for associated matrix displacements:

$$U_M(\sigma) = \frac{\sigma.\ell_d}{E_M.(1-V_F)}.\frac{a.(1-\beta)}{2.(1+a)}. \tag{2.9}$$

The difference between fiber elongation (Equation (8)) and matrix displacement (Equation (9)) provides the matrix crack opening $2u$:

$$u = (U_F - U_M) = \frac{\sigma.\ell_d}{E_F.V_F - \sigma}.\frac{(1+\beta)}{2}. \tag{2.10}$$

In the presence of n matrix cracks, microcomposite elongation ($U_T(n,\sigma)$) is the sum of fiber elongations in the debonded regions (U_F) and in the intact region (U_{int}).

$$U_T(n,\sigma) = U_{\text{int}}(L - 2.n.(l_d+u)) + 2.n.U_F, \tag{2.11}$$

where L is microcomposite length.

Inserting the expressions of U_{int} and U_F into Equation (11), $U_T(n,\sigma)$ can be expressed in the following simple manner:

$$U_T(n,\sigma) = \frac{\sigma}{E_0}.L.\left[1 + \frac{2.n.\ell_d.a}{L}\left(1 + \frac{\sigma}{E_F V_F - \sigma}\right)\frac{(1+\beta)}{2}\right] \tag{2.12}$$

where E_0 is the initial Young's modulus of microcomposite.

Considering that elongations remain essentially small ($L \approx L_0$, L_0 is the initial length of microcomposite), microcomposite strain, ε_T and Young's modulus, E, in the presence of n matrix cracks were derived from equation (12):

$$\varepsilon_T = \frac{\sigma}{E_0}.\left[1 + \frac{2.n.\ell_d.a}{L_0}.\left(\frac{\sigma}{E_F V_F} + 1\right)\frac{(1+\beta)}{2}\right], \tag{2.13}$$

$$E = \frac{E_0}{1 + \frac{2.n.\ell_d.a}{L_0}.\left(\left(\frac{\sigma}{E_F V_F - \sigma} + 1\right)\frac{(1+\beta)}{2}\right)}. \tag{2.14}$$

Equations (13) and (14) require the number n of matrix cracks as a function of the applied stress σ. Determination of n as a function of σ is based upon strength-probability equations.

2.3. STRENGTH-PROBABILITY EQUATIONS

Formation of a new crack in the matrix results from the brittle failure of an uncracked matrix fragment. Occurrence of a single crack in a matrix fragment causes its failure perpendicular to the fiber. The fragment is thus split into two new fragments.

Matrix cracking can be described by applying weakest link statistics to the brittle failure of each fragment.

The probability of failure of the fragments and the fiber was derived from the following 2-parameter simple Weibull's equation for volume-located fracture origins:

$$P = 1 - \exp\left[-\int\left(\frac{\sigma}{\sigma_0}\right)^m .\mathrm{d}V\right]. \tag{2.15}$$

σ refers here to the stresses in the fiber or the matrix (σ_F and σ_M respectively) rather than to the stress in the composite; m and σ_0 are the statistical parameters.

In the presence of n matrix cracks, the matrix is subdivided into $(n+1)$ fragments (Figure 6). The probability of brittle failure of the ith matrix fragment of length $2l_i$ is given by the following equation:

$$P_{Mi} = 1 - \exp\left[-2S_M.\int_0^{\ell i}\left(\frac{\sigma_M}{\sigma_{0M}}\right)^{m_M}.\mathrm{d}x\right], \tag{2.16}$$

where S_M is the cross-sectional area and m_M and σ_{0M} are the statistical parameters pertinent to the matrix. σ_M in Region 2 of matrix fragments, is given by equation (4). σ_M in Region (3) is uniform: $\sigma_M = (\sigma a/V_M(1+a))$.

Incorporating the appropriate equations for σ_M and integrating equation (16) gives:

$$P_{Mi} = 1 - \exp\left[-2S_M.\left(\frac{\sigma}{\sigma_{0M}}.\frac{a}{V_M.(1+a)}\right)^{m_M}.\left[\ell_i - \frac{\ell_{di}}{(m_M+1)}.(m_M+\beta)\right]\right], \tag{2.17}$$

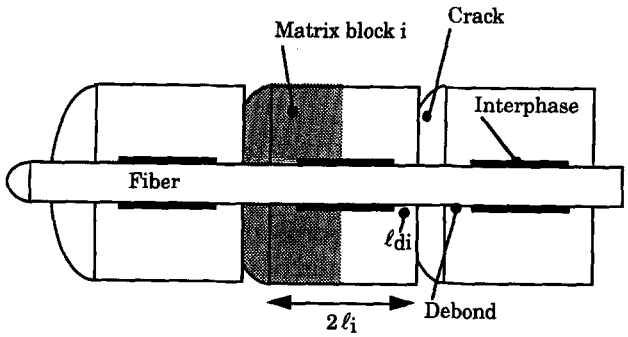

Figure 6. Schematic diagram showing the fragments created by matrix cracks in a microcomposite.

where l_{di} is the debond length in ith matrix fragment.

This approach implicitly assumes that a single population of flaws is responsible for matrix cracking, and that the Weibull equation still describes scale effects as fragments become shorter and shorter. The plots in Figure 4 and the Weibull moduli obtained at successive crack steps [4] indicate that the flaw strength parameters are not affected by small numbers of cracks. Other failure probability equations, such as the Weibull one as modified by Phani [23], could be used for larger numbers of cracks.

The strength σ_M^i of the ith matrix fragment of volume V_i is derived from equation (17). It may be expressed as a function of a reference matrix strength σ_M^R which measures the strength of the initial volume of matrix (V_{OM}) is the uncracked microcomposite:

$$P_{MO} = 1 - \exp\left[-V_{OM} \cdot \left(\frac{\sigma_M^R}{\sigma_{OM}}\right)^{m_M}\right]. \tag{2.18}$$

Equating P_{Mi} and P_{MO} gives σ_M^i:

$$\sigma_M^i = \sigma_M^R \left(\frac{V_{OM}}{V_i}\right)^{1/m_M} \left(1 - \frac{l_{di}}{l_i}\frac{m_M + \beta}{m_M + 1}\right)^{-1/m_M}. \tag{2.19}$$

It may be considered that the ith fragment fails when the stress acting on the matrix (σ_M) exceeds the fragment strength. A criterion for the formation of a crack is thus:

$$\sigma_M^i \leqslant \sigma_M.$$

The evolution of the number of matrix cracks versus stress which can be derived using equation (19), depends on fragment lengths $2l_i$. A simple approximation of the matrix strength at saturation may be obtained by considering the average crack spacing at saturation ($2l_n = (L_0/n)$) and assuming that the debonds extend over the entire microcomposite length ($l_d = l_n$):

$$\sigma_M^S = \sigma_M^R [n(m_M + 1)]^{1/m_M}. \tag{2.20}$$

A similar approach was applied to determine the failure probability of the fiber in the presence of matrix cracks. For a single matrix crack, the failure probability of the fiber may be calculated from the following equation assuming a volume-located failure origin:

$$P_F(1) = 1 - \exp[-2S_F \int_0^L \left(\frac{\sigma_F}{\sigma_{OF}}\right)^{m_F} \mathrm{d}x], \tag{2.21}$$

where S_F is the cross-sectional area of the fiber, m_F and σ_{OF} are the statistical parameters pertinent to the fiber and σ_F is the stress acting over the fiber.

Incorporating Equations (3) and (5) for σ_F and integrating equation (21) by considering that the fiber consists of $(n+1)$ volume elements associated to the matrix fragments, leads to the following equation for the failure probability of the fiber in the presence of n matrix cracks:

$$P_F^T(n) = 1 - \exp\left[-\left(\frac{\sigma}{\sigma_{OF}}\frac{1}{V_F(1+a)}\right)^{m_F} V_{OF}\left[2n\frac{l_d}{L}A + 1\right]\right], \tag{2.22}$$

where

$$A = \left(\left(\frac{u}{l_d} + \beta\right)(1+a)^{m_F} - \frac{1-\beta}{m_F+1}\left(\frac{1-(1+a)^{m_F+1}}{a}\right) - 1\right).$$

The effective volume of fiber $V_F^E(n)$ which gives the same failure probability under the uniformly distributed stress σ_F is:

$$V_F^E(n) = \frac{V_{OF}}{(1+a)^{m_F}}\left[1 + 2n\frac{l_d}{L}A\right]. \tag{2.23}$$

The failure stress of the fiber in the presence of n matrix cracks $\sigma_F(n)$ may be related to the reference fiber strength the σ_F^R defined as the initial strength of the single fiber (length L_0) under uniform tensile loading. This relation is obtained by equating the failure probability of the microcomposite (Equation (22)) and the failure probability of a single fiber under uniform tension:

$$\sigma_F(n) = \sigma_F^R\left[\frac{V_{OF}}{(V_F^E)}\right]^{1/m_F} \equiv \sigma_F^R\frac{(1+a)}{(1+2n\frac{ld}{L_0}A)^{1/m_F}}. \tag{2.24}$$

3. Application to SiC/SiC microcomposites

3.1. Simulation of matrix cracking

The determination of the number of matrix cracks as a function of the applied stress is based on the strengths of matrix fragments (Equation (19)) and on the failure criterion: $\sigma_M^i \leqslant \sigma_M$.

The matrix strength data exhibit a statistical distribution. The mean strengths were used in the analysis. Therefore, the average behavior of a batch of microcomposites was computed.

The debond length l_{di} is given by Equation (6). An explicit equation of the evolution of l_i is not available yet. l_i was determined by using an iterative procedure.

Formation of matrix fragments is dictated by the distributions of flaws. Fragment lengths depend on the location of the fracture-inducing flaws. Fragment lengths may be regarded as statistical data. They were derived from the probability (λ_i) of location of the critical defect in the fragment: $\lambda_i = l_j/2l_i$, where l_j indicates the location of the critical flaw (i.e. the distance from the matrix crack plane), and $2l_i$ is the fragment length. Therefore, the lengths of both matrix fragments created at step i by the failure of a fragment of length $2l_i$ are respectively $2\lambda_i l_i$ and $2(1-\lambda_i)l_i$. The λ_i data were computer generated random numbers $(0 < \lambda i < 1)$.

Initiating this procedure for the uncracked cylinder of matrix (length L_0, volume V_{OM}) allows the iterative determination of the successive fragment lengths as σ increases, and therefore the use of Equation (19) for the computation of cracking stresses.

The simulation of matrix fragmentation may be summarized as follows. The first crack is created when the stress operating on the matrix σ_M exceeds the mean matrix strength for the initial volume V_{OM}. The lengths of the resulting fragments are respectively:

$$l_1 = 2\lambda_1 L_0 \quad \text{and} \quad 1'_1 = 2L_0(1 - \lambda_1).$$

The corresponding fragment strengths σ_1 and σ'_1 are derived from the reference matrix strength using Equation (19). Stress for the formation of the second crack is $\sigma_M = \sigma_1$ (assuming for simplicity that $\sigma'_1 > \sigma_1$). The σ_1-fragment is subdivided into two new fragments of lengths $l_2 = 2\lambda_2 l_1$ and $l'_2 = 2(1 - \lambda_2)l_2$. The fragment strengths σ_2 and σ'_2 are derived from Equation (19). The formation of the third crack occurs when σ_M exceeds the lowest fragment strength $(\sigma'_1, \sigma_2, \sigma'_2)$. The procedure is repeated unless one of the following conditions is no longer satisfied:

(i) fragment strengths are smaller than the corresponding fiber strength given by Equation (24),

(ii) debond length (Equation (6)) within the critical matrix fragment at each step does not exceed fragment length:

$$2l_{di} \leqslant 2l_i.$$

As soon as this second condition is no longer fulfilled, it is considered that saturation of matrix cracking occurred. The mechanical behavior of the microcomposite becomes dominated by the fiber. Ultimate failure occurs when the fiber strength (Equation (24)) is smaller than the stress applied to the fiber.

Computations were performed at a constant debond length l_d and also for debond lengths growing with the applied stress, according to Equation (6). Simulation of the matrix cracking process is illustrated in Figure 7 which shows the distribution of cracks at saturation for various debond lengths. Matrix cracking was allowed in the region surrounding interfacial debond only in Figure 7c.

3.2. MICROCOMPOSITE PROPERTIES

The mean characteristics of the SiC/SiC microcomposites (Table 1) that were used for the computations were measured in a previous paper [4]. The statistical parameters pertinent to the SiC matrix deposited by CVI, were estimated from the statistical distributions of stresses at the onset of matrix cracking measured in batches of SiC/SiC microcomposites of various lengths [4].

Figure 4 shows an example of the statistical distributions of matrix strength data determined on a batch of SiC/SiC microcomposites (10 mm gauge length). The strength data were derived from the applied forces at the formation of matrix cracks, identified by acoustic emission and using features of the load-displacement curves shown in Figure 3. The strength data at each crack were treated using the ranking statistics method and were ordered from lowest to largest.

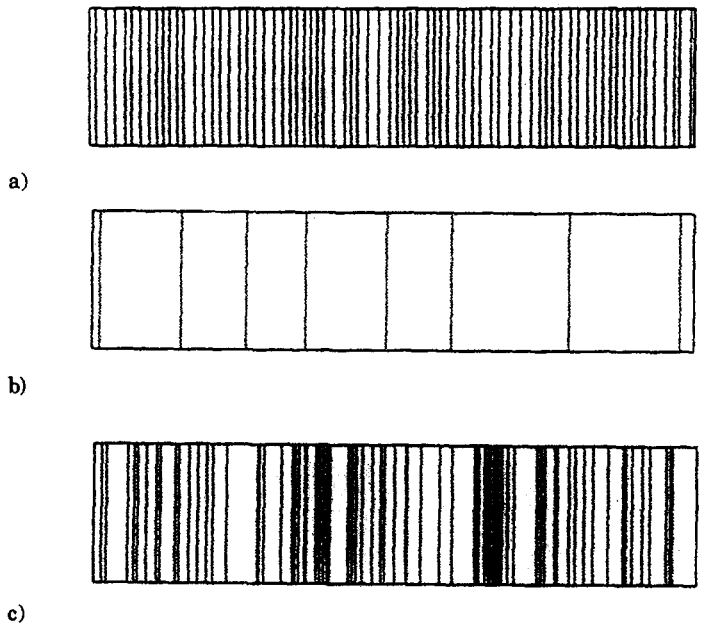

Figure 7. Simulated matrix crack distributions at saturation for short debonds ((a) and (c): $l_d/L = 0,0125$) and for long debonds ((b): $l_d/L = 0,125$). In (c) formation of cracks was allowed in the portions of matrix adjacent to debonds.

Table 1. Mean characterisitics of the tested SiC/SiC microcomposites (scatter is indicated in brackets) [4].

V_F	0.26 [0.16–0.41]
E_M	300 GPa
E_F	180 GPa
m_M	4.9
m_F	3.9
$\sigma_{OM}(V_O = 1\ \text{m}^3)$	3 MPa
$\sigma_{OF}(V_O = 1\ \text{m}^3)$	2.5 MPa
L_0	10 mm
$\tilde{\sigma}_M$	589 MPa
$\tilde{\sigma}_F$ (25 mm)	2200 MPa
d_F	15 μm [10–20]
Number of cracks at saturation	3 [1–5]
Debond lengths	1.6 mm [1–2]
Number of test specimens	13

Then, the failure probability P_j was associated to the jth data using the following estimator:

$$P_j = \frac{j - 0,5}{N}, \tag{26}$$

where N is the total number of the stress data at each step of cracking.

Table 2. Mean matrix cracking stresses (MPa) predicted for the SiC/SiC microcomposites tested in this paper.

		First crack	Second crack	Third crack
Experimental	Mean strengths	589	671	749
	$P_j(n) = 0.5$	582	649	749
Predictions	constant $l_d = 1.66\,\mu m$	564	619	705
	stress dependent l_d: $\tau_0 = 5$ MPa	564	611	699

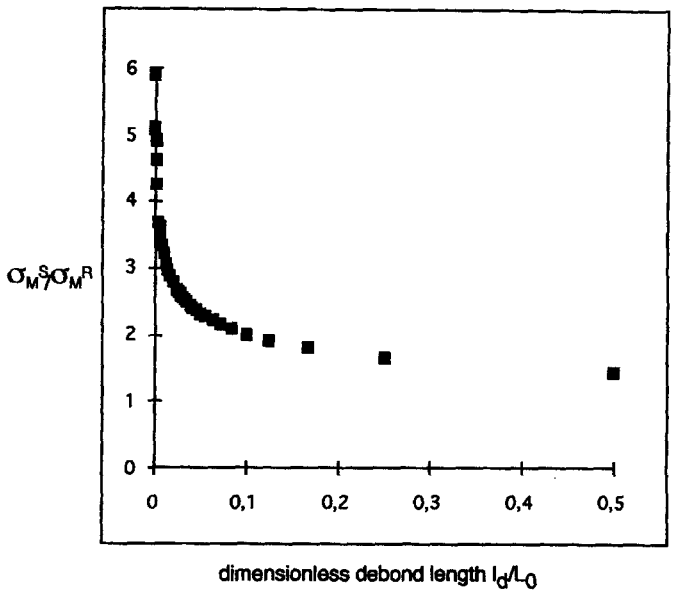

Figure 8. Prediction of the influence of debond length on the stress at saturation for a SiC/SiC microcomposite (for a uniform distribution of matrix cracks at saturation).

4. Results and discussion

4.1. Matrix cracking stresses

Table 2 gives the mean matrix cracking stresses predicted for the batch of SiC/SiC microcomposites examined here. The predictions agree with the experimental data. The slight discrepancy which is observed between predictions and experiments must be attributed to the inherent uncertainty and variability in certain characteristics (including l_d, τ_0, statisitical parameters, etc.).

The results also show that the propagation of debond did not significantly influence matrix cracking for the range of debond lengths which was considered here ($l_d \geqslant 1$ mm). However, it can be noticed that, as logically expected, interfacial crack growth may cause fragment strength decrease.

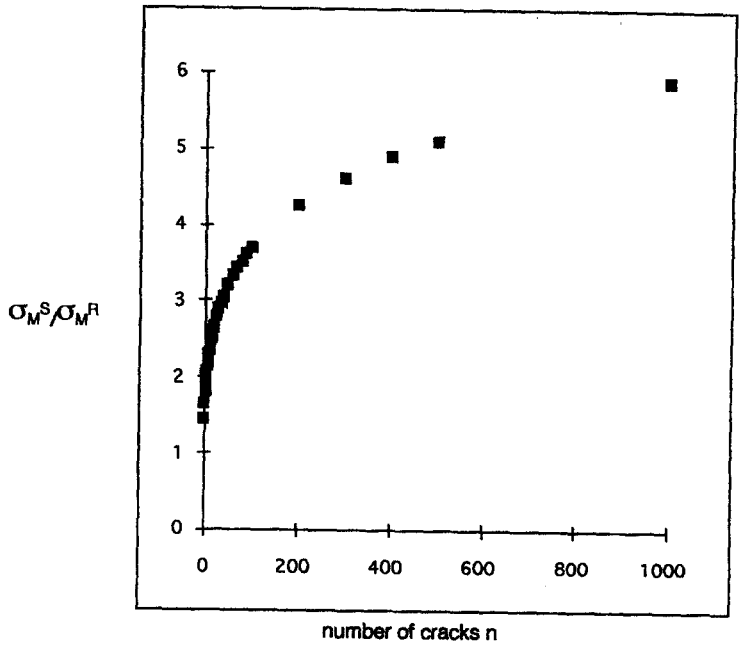

Figure 9. Prediction of the dependence of the stress at saturation on the number of matrix cracks, for SiC/SiC microcomposites (for a uniform distribution of matrix cracks).

4.2. FEATURES OF THE STRESS–STRAIN BEHAVIOR

Features of the stress–strain behavior, including the stress at saturation and ultimate failure were calculated for various debond lengths using Equations (20) and (24). It will be noticed from Figures 8 and 9 that the stress at saturation σ_M^S is strongly affected by the debond length and by the associated number of cracks. High stresses at saturation require short debonds whereas the numbers of associated matrix cracks are large. Theory predicts that matrix strength at saturation can reach infinity in the presence of very short debonds. Obviously, at this stage, matrix cracking becomes limited by fibre fracture. On the basis of the mean reference strengths for the fiber and the SiC matrix given in Table 1 and taking into account the scale effects (Equation (24)), an average maximum value of around 5 may be estimated for σ_M^S/σ_M^R for the SiC/SiC microcomposites. It is worth mentioning that this limit may be affected by fiber degradation during processing. Figures 8 and 9 thus allow the estimation of the debond length and the associated number of cracks required to reach the maximum saturation stress. For the SiC/SiC microcomposites examined here ($\sigma_M^S/\sigma_M^R = 5$), the following requirements were estimated: $l_d/L_0 \approx 0.001, l_d = 10\,\mu$m for $L_0 = 10$ mm and $n = 400$. Below this debond length, saturation is dictated by fiber strength. Higher stresses at saturation require stronger fibers.

Equations (20) and (24), can also be used to anticipate the influence of preponderant fiber and matrix properties on the stress at saturation and at ultimate failure.

Figure 10 shows that the microcomposite ultimate failure depends strongly on the total debond length $2nl_d$. High strengths coincide with short debonds. Such improvement of load bearing capabilities through strong fiber/matrix interactions is in agreement with experimental observations. Long debonds lower microcomposite strengths which is indicative of fiber

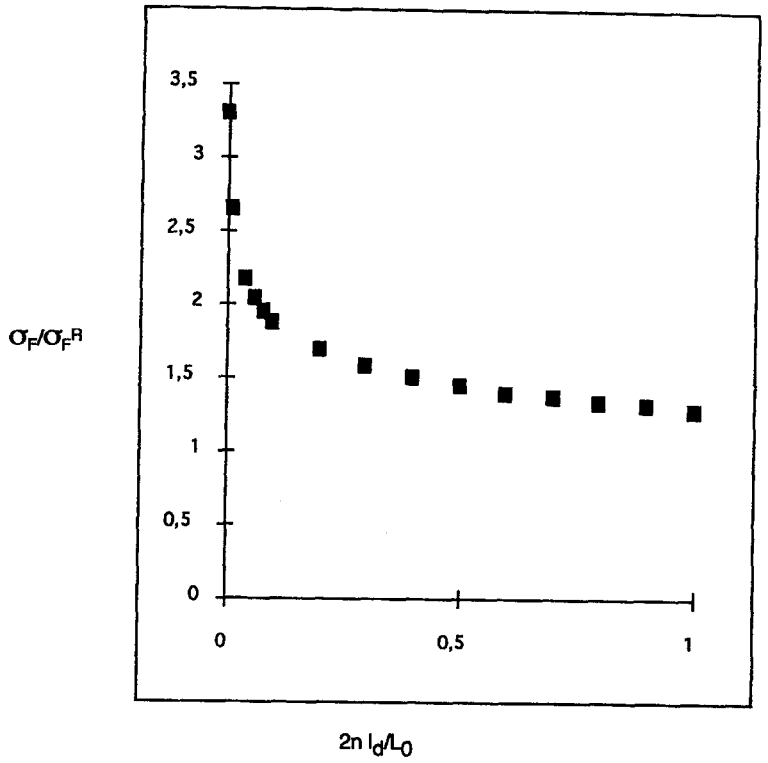

Figure 10. Prediction of the effect of total debond length on ultimate failure of SiC/SiC microcomposites.

weakening by overloading. The debond growth is observed in fatigue. Lifetime in fatigue is determined by debond-induced fiber overloading.

Fiber weakening due to matrix cracking or debond growth is also reflected by the effective volume $V_F^E(n)$ (Equation (23)). Computations show that $V_F^E(n)$ is initially significantly smaller than fiber volume, which reflects the contribution of the matrix to load bearing.

The above results highlight the influence of interfaces on the saturation stress, the microcomposite strength and the associated number of matrix cracks. The debond length reflects the magnitude of fiber/matrix interactions. Short debonds are indicative of strong interactions and long debonds of weak interactions. The above predictions show that strong fiber/matrix interactions enhance matrix cracking and improve, the microcomposite strength. Matrix cracking saturation tends to be dictated by the fiber, therefore, it tends to be coincident with microcomposite strength. This implies the presence of a wide non-linear domain of deformations and a large number of matrix cracks. By contrast, microcomposite strength and the stress at saturation are smaller in the presence of weak fiber/matrix interactions, and they are distinct, leading to a narrow non-linear domain of deformations and a smaller number of matrix cracks. The same features are observed on practical CMCs (Figure 1). For comparison purposes, rough estimates of fiber/matrix interactions and the extent of matrix cracking may be obtained from the simple inspection of the stress–strain curves measured under tensile loads.

The use of the Weibull equation may lead to an overestimation of matrix strengths as fragments become shorter and shorter, thus leading to an underestimation of the number of cracks. For Carbon fibers, the discrepancy between the measured strengths and Weibull's equation-based predictions tends to be significant for lengths more than hundred times shorter

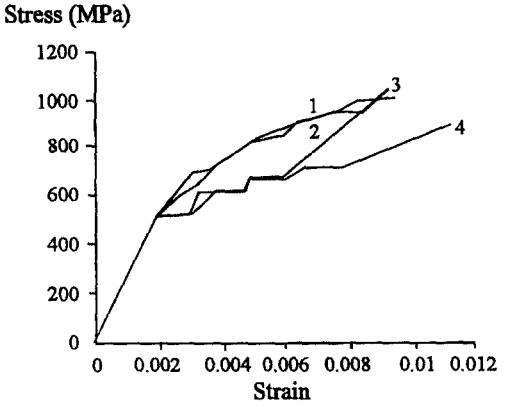

Figure 11. Prediction of the influence of debond length upon the stress–strain curves for SiC/SiC microcomposites ($\beta = 0; k = 0$): (1) $l_d = 0.1$ mm, constant debond ($\tau_0 = 100$ MPa), (2) $l_d = 0.1$ mm, growing debond ($\tau_0 = 100$ MPa), (3) $l_d = 1$ mm, constant debond ($\tau_0 = 10$ MPa), (4) $l_d = 1$ mm, growing debond ($\tau_0 = 10$ MPa).

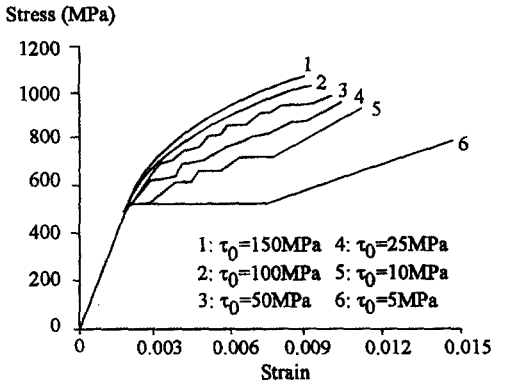

Figure 12. Influence of interfacial shear stress upon stress strain curves for SiC/SiC microcomposites ($\beta = 0$; $k = 0$).

than the initial length [23]. On the basis of these results it may be foreseen that matrix strength overestimations may become significant for fragment lengths smaller than 100 μm and the associated numbers of matrix cracks larger than 100 (for $L_0 = 10$ mm). Therefore, the number of matrix cracks may be underestimated for large numbers of cracks and for those microcomposites with very strong interphases. This will not affect the trends predicted in paper.

STRESS–STRAIN CURVES

The computed stress-strain curves (Figures 11–14) agree with those measured on practical SiC/SiC microcomposite specimens: they exhibit comparable ranges of stresses and strains.

Figures 11–14 confirm the above conclusions on the influence of fiber/matrix interactions through interfaces upon the stress–strain curves, which may be summarized as follows: strong fiber/matrix interactions favor matrix cracking, high stresses and a high stress at saturation which tends to coincide with the ultimate strength. Let's examine now the influence of the different interfacial characterisitics defined in the previous section.

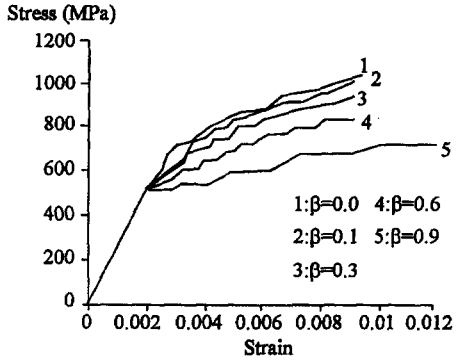

Figure 13. Influence of the β parameter upon the stress–strain curves for SiC/SiC microcomposites (τ_0 = 150 MPa; $k = 0$).

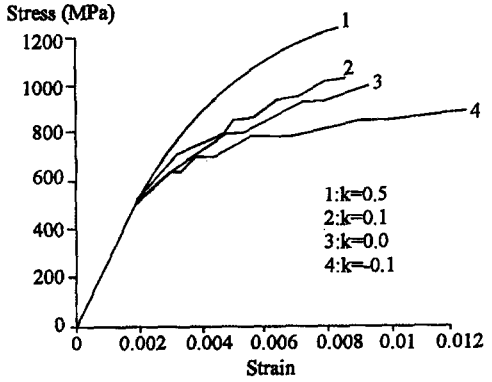

Figure 14. Influence of the k parameter upon the stress–strain curves for SiC/SiC microcomposites ($\beta = 0$; τ_0 = 150 MPa).

Figure 11 describes the influence of debond length. As previously mentioned, the stress–strain curves exhibit a wide non-linear domain and a high stress at saturation coincident with the ultimate strength when the debond is short (rather strong fiber/matrix interactions: τ_0 = 100 MPa). By contrast, the non-linear domain appears more narrow and the stress at saturation tends to be much lower than ultimate strength when the debond is long (rather weak fiber/matrix interactions: τ_0 = 10 MPa).

Finally, it can be noticed from Figure 11 that the propagation of interfacial debond significantly affects the stress–strain curves only in the presence of weak fiber/matrix interactions ($\tau_0 \leqslant 10$ MPa). This result is in agreement with logical expectation.

Figure 12 shows the dependence of the stress–strain behavior on the interfacial shear stress. The trends previously discussed and evidenced by Figure 11 are confirmed. The results are in agreement with the experimental data obtained on practical 2D woven SiC/SiC CVI-composites. Thus, for those CMC exhibiting a plateau-like behaviour, low τ_0 were estimated (< 10 MPa) [24, 25]. In contrast, significantly larger τ_0(> 100 MPa) have been measured on those composites exhibiting higher stresses, a wide non-linear domain of deformations and a stress at saturation close to ultimate failure [24].

Figure 13 describes the influence of the distance along which fiber/matrix interactions are effective. When fiber/matrix interactions operate over a significant distance (rather significant

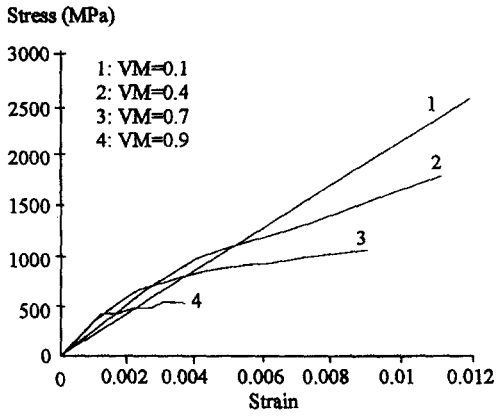

Figure 15. Influence of the volume fraction of matrix upon the stress–strain curves for SiC/SiC microcomposites ($\tau_0 = 150$ MPa).

interactions) $\beta(= l_0/l_d)$ is low. Interactions along a short distance are characterized by large values of β (weak interactions). Figure 13 confirms the previously mentioned trends. Non-linearity and high stresses are favoured by very small β values. A plateau-like behavior and a low stress at saturation are obtained for large β values.

Figure 14 shows the influence of radial compression or tension on the interface, as accounted for by coefficient k. The predicted stress–strain curves confirm the previously discussed trends. Higher stresses and a wide non-linear domain are obtained when the interface is under significant compression ($k > 0$). Decreasing k towards negative values (the interface tends to be under tension) diminishes the stresses. The stress–strain behavior tends to be characterized by a plateau-like curve.

Figure 15 predicts the influence of the volume fraction of the matrix on the stress–strain curves for a microcomposite possessing a rather strong interface ($\tau_0 \approx 150$ MPa). Results show that the features of the stress–strain curves are tremendously affected when the volume fraction of matrix is modified around the reference value of 0.7. Reduction of the volume fraction of the matrix causes the behavior to be increasingly dominated by the fiber, leading to higher stresses and strains. For large volume fractions of matrix, the initiation and saturation of matrix cracking occurs at low stresses and strains. These trends reflect scale effects.

The above trends are in agreement with the data available in the literature and with the stress–strain behaviors measured on various practical 2D SiC/SiC composites and microcomposites. Phoenix [26] anticipated that increases in τ_0 lead to a reduction in the matrix crack spacing in brittle matrix fibrous composites. Curtin predicted the same effect of τ_0 on the fiber characteristic strength and on the ultimate tensile strength in unidirectional CMCs [12]. The predicted influence of the volume of matrix on the stress at the onset of matrix cracking has been observed in microcomposites [22] and in CMCs [27]. As previously mentioned the highest stresses at saturation and at ultimate failure have been observed on CMCs possessing the strongest interphases [24, 25, 27]. The largest numbers of cracks at saturation have been detected in the presence of strong fiber/matrix interactions [25].

For reasons of simplicity, the axial thermally induced residual stresses were not incroporated in the stress–strain equations. However they were taken into account in the simulation of matrix cracking through the experimental value of σ_M^R (Table 1). The influence of the radial residual stresses is incorporated in the equation proposed for τ. The direct determination of

thermally-induced residual stresses is not straightforward, owing to a result of a big uncertainty in the thermoelastic properties available for the fiber, the carbon interphase and the CVI-SiC matrix.

Conclusions

An approach to the relationships existing between interfacial parameters and the stress–strain behavior was proposed for microcomposites. Stress–strain relations were derived from fiber elongations in the regions delineated by matrix cracking and debonding.

A Weibull type statistical-probabilistic model was developed for the description of the matrix cracking process and fiber failure. This model provided stress-probability equations as a function of the number of matrix cracks and interfacial parameters. The interfacial parameters included debond length (l_d), interfacial shear stress (τ_0), and stress dependent fiber/matrix interactions involving Poisson's effect, friction and residual stresses.

This approach was applied to SiC/SiC microcomposites. The predicted matrix cracking stresses were found to be in excellent agreement with the data measured on a batch of SiC/SiC microcomposites.

Predictions of the stress-strain curves as well as features of the stress–strain behavior as a function of interfacial parameters evidenced various trends which are readily observed on practical microcomposites and CMCs. Predictions thus showed that strong fiber/matrix interactions (as measured by short interfacial debonds (l_d), large interfacial shear strength (τ_0), limited Poisson's effect ($l_0 \ll l_d$), and significant radial compression ($k > 0$)) favor matrix cracking, high stresses and a high stress at saturation which tends to coincide with ultimate failure. In the presence of weaker interfaces, stresses are low, the nonlinear domain of deformations is narrow, and the stress at saturation is significantly smaller than ultimate strength. The growth of interfacial debond significantly affected the stress–strain curve only in the presence of weak interfaces.

Therefore, observation of the above features on the stress–strain behavior of CMCs, allows a rough estimate of the importance of fiber/matrix interactions.

The analysis indicated that the stress–strain behavior involves scale effects. The influence of interfacial properties operate through the stress field acting on the matrix fragments and on the fiber. Fragmentation improves matrix strength and degrades fiber efficiency and the interfacial debond dictates the stresses acting on the fragments. In the presence of strong interfaces, larger volumes of matrix are stressed, which causes more significant cracking when compared with weak interphases. The fiber strength depends on the total debond length ($2nl_d$).

The model provided the relationships between the four basic criteria for damage and failure in CMCs: stresses, failure probability, debond length (or interfacial shear stress), and the number of matrix cracks. We can go around this square in any way to predict a given set of data. For instance, we can predict reliability as a function of applied stresses and interfacial characteristics. We can also derive interfacial characteristics from applied stresses and the number of matrix cracks. Therefore, this model provides a tool for extracting interfacial characteristics from the stress–strain curves measured on microcomposites.

Acknowledgements

The authors acknowledge the support of SEP and CNRS through a grant given to L. Guillaumat.

References

1. H.C. Cao, E. Bischoff, O. Sbaizero, Manfred Rühle, A.G. Evans, D.B. Marshall and J.J. Brennan, Effect of interfaces on the properties of fiber-reinforced ceramics. *Journal of American Ceramic Society* 73(6) (1990), 1691–99.
2. R. Naslain, Fiber-matrix interphases and interfaces in ceramic matrix composites processed by CVI. Composites Interfaces, Vol 1, n° 3, 1993 pp. 253–286.
3. J. Lamon, Interfaces and Interfacial Mechanics: Influence on the Mechanical Behavior of Ceramic Matrix Composites (CMC). Journal de Physique IV, colloque C7, supplement au Journal de Physique III, volume 3, (novembre 1993) 1607–1616.
4. J. Lamon, N. Lissart, C. Rechigniac, D.M. Roach, J.M. Jouin, 'Micromechanical and Statistical Approach to the Behavior of CMCs' pp 1115–1124 in Composites and Advanced Ceramics, Proceedings of the 17th Annual Conference and Exposition, (10–15 jan. 1993-Cocoa Beach, Florida (USA). Ceramic Engineering and Science Proceedings, September-October 1993, The American Ceramic Society.
5. C. Droillard, Elaboration et caractérisation de composites à matrices SiC et à interphase séquencée SiC/C-Ph.D. Thesis, n° 913, University of Bordeaux, June 1993.
6. J. Aveston, G.A. Cooper and A. Kelly, Single and Multiple Fracture, pp 15–26 in 'The Properties of Fiber Composites' Conference Proceedings of the National Physical Laboratory, IPC Science and Technology Press, Surrey, England, (1971).
7. B. Budiansky, J.W. Hutchinson and A.G. Evans, Matrix fracture in fiber-reinforced ceramics. *Journal of Mechanical Physics and Solids*, 34 (1986) 167–189.
8. D. Marshall, B. Cox and A.G. Evans, The mechanics of matrix cracking in brittle-matrix fiber composites. *Acta Metallurgica* 33 (1985) 2013–2021.
9. L.N. McCartney, Mechanics of matrix cracking in brittle-matrix fiber-reinforced composites. *Proceeding of Royal Society of London*, A.409 (1987) 329–350.
10. M.D. Thouless and A.G. Evans, Effects of pull-out on the toughness of reinforced ceramics. *Acta Metallurgica* 36 (1988) 517.
11. M.D. Thouless, O. Sbaizero, L.S. Sigl and A.G. Evans, Effects of interface mechanical properties on pull-out in a SiC-fiber-reinforced lithium aluminium silicate glass ceramic. *Journal of American Ceramic Society* 72 (1989) 525.
12. W.A. Curtin, Theory of mechanical properties of ceramic matrix composites. *Journal of American Ceramic Society* 74 [11] (1991) 2837–2845.
13. P.S. Steif and H.R. Schwietert, Ultimate strength of ceramic matrix composites. *Ceramic Engineering Science Proceedings* 11 [9–10] (1990) 1567–1576.
14. M. Sutcu, Weibull statisitics applied to fiber failure in ceramic composites and work of fracture. *Acta Metallurgica* 37 (1989), 2567–83.
15. H. Cao and M.D. Thouless, Tensile tests on ceramic-matrix composites: Theory and experiment. *Journal of American Ceramic Society* 73 [7] (1990) 2091–94.
16. J.D. Achenbach and H. Zhu, Effect of interfacial zone on mechanical behavior and failure of fiber reinforced composites. *Journal of Mechanical Physics and Solids* 37 (1989) 381.
17. A.W. Pryce and P.A. Smith, Matrix cracking in unidirectional ceramic matrix composites under quasi-static and cyclic loading. *Acta Metallurgica Material* 41 [4] (1993) 1269–1281.
18. J. Lamon, C. Rechiniac, N. Lissart, P. Corne, 'Determination of Interfacial Properties in Ceramic Matrix Composites using Microcomposites specimens' pp 585–590 in Proc. Fifth European Conference on Composite Materials (ECCM V Bordeaux) Edited by A.R. Bunsell, J.F. Jamet, and A. Massiah, EACM, Bordeaux 1992.
19. J. Lamon and L. Guillaumat, 'A Probabilistic Approach to the Failure of Ceramic Matrix Composites: Analysis of the influence of Fiber/Matrix Interfaces' Ibid. 18, 895–900.
20. P. Corne, C. Rechiniac and J. Lamon, 'An approach to fiber/matrix debond resistance in microcomposites' (une approche de la résistance de la décohésion fibre/matrice dans les microcomposites à matrice céramique) pp. 213–224 in Comptes Rendus des 8èmes Journées Nationales sur les Matériaux Composites (JNC8; Paris, Nov. 1992), Edited by O. Allix, J.P. Favre et P. Ladevèze, AMAC, Paris, 1992.
21. J.L. Bobet and J. Lamon, Thermal residual stresses in ceramic matrix composites. *Acta Metallurgica Materials* 43 [6] (1995) 2241–2253.
22. J. Lamon, F. Rebillat, A.G. Evans, Assessment of a microcomposite test procedure for evaluating constituent properties of ceramic matrix composites. *Journal of American Ceramic Society* 78 [2] (1995) 401–405.
23. K.K. Phani, The strength-length relationship for carbon fibers. *Composites Science and Technology* 30 (1987) 59–80.
24. C. Droillard, P. Voisard, C. Heibst and J. Lamon, Determination of fracture toughness in 2D-woven SiC matrix composites made by chemical vapor infiltration. *Journal of American Ceramic Society* 78 [5] (1995) 1201–11.

25. C. Droillard, J. Lamon, Fracture toughness of 2D woven SiC/SiC CVI-composites with multilayered interphases. *Journal of American Ceramic Society* 79 (1996), 849–58.
26. S.L. Phoenix, Statistical issues in the fracture of brittle-matrix fibrous composites. *Composites Science and Technology* 48 (1993), 65–80.
27. L. Guillaumat, 'Multifissuration des CMC: Relation avec la microstructure et le comportement mécanique' (Multiple Matrix Cracking in CMC: Relations with Microstructure and Mechanical Behavior). Ph. D. Thesis, n° 1056, University of Bordeaux, February 1994.